Energy loss of leading hadrons and direct photon production in evolving quark-gluon plasma

Simon Turbide,[1] Charles Gale,[1] Sangyong Jeon,[1,2] and Guy D. Moore[1]
[1]*Department of Physics, McGill University, 3600 University Street, Montreal, Canada H3A 2T8*
[2]*RIKEN-BNL Research Center, Upton, New York 11973-5000, USA*
(Received 7 March 2005; published 18 July 2005)

We calculate the nuclear modification factor of neutral pions and the photon yield at high p_T in central Au-Au collisions at the Relativistic Heavy-Ion Collider (RHIC) ($\sqrt{s} = 200$ GeV) and Pb-Pb collisions at the Large Hadron Collider (LHC) ($\sqrt{s} = 5500$ GeV). A leading-order accurate treatment of jet energy loss in the medium has been convolved with a physical description of the initial spatial distribution of jets and a one dimensional hydrodynamic expansion. We reproduce the nuclear modification factor for pions R_{AA} at RHIC, assuming an initial temperature $T_i = 370$ MeV and a formation time $\tau_i = 0.26$ fm/c, corresponding to $dN/dy = 1260$. The resulting suppression depends on the particle rapidity density dN/dy but weakly on the initial temperature. The jet energy loss treatment is also included in the calculation of high p_T photons. Photons coming from primordial hard N-N scattering are the dominant contribution at RHIC for $p_T > 5$ GeV, whereas at the LHC, the range $8 < p_T < 14$ GeV is dominated by jet-photon conversion in the plasma.

DOI: 10.1103/PhysRevC.72.014906 PACS number(s): 25.75.−q, 12.38.Mh

I. INTRODUCTION

One of the most important issues that arises in the study of relativistic heavy-ion collisions is that of the creation of a quark-gluon plasma (QGP). From lattice quantum chromodynamics (QCD) calculations, there is strong evidence that at around a temperature of 170 MeV, or equivalently an energy density of about 1 GeV/fm^3 [1], there should be a phase transition between an ordinary confined hadronic matter phase and a QGP phase, with an associated change in the relevant degrees of freedom. At the Relativistic Heavy Ion Collider (RHIC), measurements support the assertion that the initial energy density of the *created* system reaches up to 5 GeV/fm^3. However, this does not necessarily imply the creation of a QGP. To make sure that a new state of matter has been formed, independent evidence is needed. One of the most striking measurements in support of the creation of hot and dense matter at RHIC is the discovery of high p_T suppression in central Au-Au collisions. This phenomenon is observed in single hadron spectra [2,3] and in the disappearance of back-to-back correlations of high p_T hadrons [4].

There are a number of factors that can potentially influence the spectrum of high p_T partons in heavy-ion collisions compared to that in hadron-hadron collisions:

(i) A difference between the parton distribution functions of a proton and a heavy nucleus. This can be both depletion (shadowing) or excess (antishadowing) depending on the value of momentum fraction x. This also includes the effect of gluon saturation.
(ii) The initial state multiple scattering effect. This is the well-known Cronin effect caused by multiple soft scatterings a parton may suffer before it makes a hard collision. This can be significant only in interactions involving nuclei.
(iii) Final state energy loss. This is because of the interaction between the produced hard parton and the hot and dense environment.

Our kinematical range of application in this work is mainly midrapidity. There, initial state effects cannot explain high p_T suppression, as otherwise such suppression should also be observed in d-Au collisions, which is not the case. High p_T suppression has to arise from a final state effect: jet energy loss [5]. On top of experimental evidence for the suppression cited above, it has been proposed [6,7] that azimuthal anisotropy at high p_T could also be explained by jet energy loss. Induced gluon bremsstrahlung, rather than elastic parton scattering, has been identified to be the dominant mechanism for jet energy loss [8,9]. In the thermal medium, a coherence effect, the Landau-Pomeranchuk-Migdal (LPM) [10] effect, controls the strength of the bremsstrahlung emission. Several models of jet quenching through gluon bremsstrahlung have been elaborated: Baier-Dokshitzer-Mueller-Peigné-Schiff (BDMPS) [11,12], Gyulassy-Levai-Vitev (GLV) [13], Kovner-Wiedemann (KW) [14], and Zakharov [15]. There have also been phenomenological studies where different energy loss mechanisms were added onto Monte Carlo jet models [16–18] (see also Ref. [19] for a recent review). In this article, we use the formalism developed by Arnold, Moore, and Yaffe (AMY) [20], which correctly treats the LPM effect [up to $O(g_s)$ corrections], to get the parton energy loss. That model will be convolved with a 1-D expanding QGP to obtain quantitative results on jet quenching. Then, the electromagnetic signature of jet-plasma interactions will be investigated.

This article is organized as follows. In Sec. II we give a qualitative description of gluon radiation and briefly review the LPM effect and the conditions for the LPM regime. In Sec. III, the AMY formalism is presented and the main distinctions between the different treatments are highlighted. In the following sections, the complete space-time evolution of the jet is calculated within a hydrodynamical model, and high p_T spectra are obtained for pions (Sec. IV) and real photons (Sec. V), for both RHIC and Large Hadron Collider (LHC) energies. Finally, Sec. VI contains a summary and conclusions.

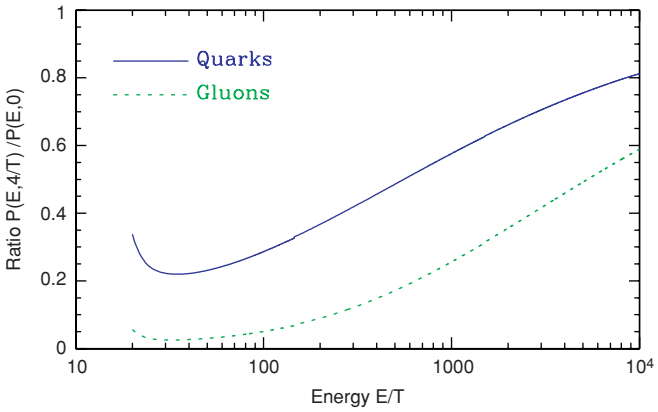

FIG. 1. (Color online) The ratio of the final over initial parton spectrum, from [23], for a representative thickness of plasma of 1.3 fermi at temperature $T = 330$ MeV, evaluated using the AMY formalism used in the current paper.

II. QUALITATIVE ARGUMENTS

The high p_T data from various RHIC experiments (see Ref. [21] for a recent review) can be characterized by the following quantity:

$$R_{AA} \equiv \frac{(dN_{AA}/dyd^2p_T)}{\langle N_{\rm coll}\rangle (dN_{pp}/dyd^2p_T)} \approx C \quad \text{for} \quad p_T \gtrsim 2\,\text{GeV}, \tag{1}$$

which represents the ratio of the number of events per unit rapidity and transverse momentum, scaled to the number expected based on proton-proton rates and the number of nuclear collisions occurring in the heavy-ion collision. As indicated, this ratio is found experimentally to be approximately constant, with the constant C ranging from about 0.2 to 0.6 depending on the centrality class and the rapidity y. The pp spectrum at midrapidity can be conveniently parametrized by [22] the following:

$$\frac{dN_{pp}}{dyd^2p_T} = A\left(\frac{p_0}{p_0 + p_T}\right)^n, \tag{2}$$

where A is a normalization constant, $p_0 = 1.2$ GeV and $n = 10$. In a previous article [23] two of us showed that the leading order thermal QCD result for energy loss, shown in Fig. 1, can qualitatively explain the fact that C is roughly constant over a finite kinematical window. In this section, we use the simple gluon radiation spectrum used by Baier *et al.* [11] to illustrate the main physical features of this calculation.

As previously stated, the dominant energy loss mechanism in medium is the radiation of gluons. We express the rate of radiation of gluons of energy ω, per unit time and ω interval, as $\Gamma \equiv dI/d\omega dt$. To understand the relationship between the behavior of R_{AA} and Γ, we note that, given Γ, the parton distribution function $P(p, t)$ (which gives the probability that there will be a parton of energy p at time t) should satisfy a rate equation,

$$\frac{dP(p,t)}{dt} = \int_{-\infty}^{\infty} d\omega P(p+\omega, t)\Gamma(p+\omega, \omega, t) - P(p,t)\int_{-\infty}^{\infty} d\omega \Gamma(p,\omega,t), \tag{3}$$

provided that conversion between different species of partons is unimportant. If the rate $\Gamma(p, \omega, t)$ has a weak dependence on p (an assumption we make here for illustration but will not use in our work in subsequent sections), then an approximate solution can be written as follows:

$$P(p,t) \approx \int d\epsilon D(\epsilon, p, t) P_0(p+\epsilon), \tag{4}$$

where

$$D(\epsilon, p, t) = \exp\left[-\int_{-\infty}^{\infty} d\omega J(p,\omega,t)\right]\sum_{n=0}^{\infty}\frac{1}{n!} \times \left[\prod_{i=1}^{n}\int_{-\infty}^{\infty} d\omega_i J(p+\omega_i, \omega_i, t)\delta\left(\epsilon - \sum_{i=1}^{n}\omega_i\right)\right] \tag{5}$$

with

$$J(p,\omega,t) \equiv \int_0^t dt' \Gamma(p,\omega,t'). \tag{6}$$

A similar expression is written down in Ref. [12]. The main difference between the current expression and the one in Ref. [12] is that the range of integration in the above equations is from $-\infty$ to ∞: The negative ω corresponds to the absorption of thermal partons and the range $\omega > p$ corresponds to annihilation of a parton with a thermal antiparton.

Following [12], we let

$$\frac{P_0(p+\epsilon)}{P_0(p)} \approx \exp(-n\epsilon/p), \tag{7}$$

which allows us to write the nuclear modification factor as follows:

$$\begin{aligned} R_{AA}(p) &= \int d\epsilon D(p,\epsilon,t)\frac{P_0(p+\epsilon)}{P_0(p)} \\ &\approx \int d\epsilon D(p,\epsilon,t)\exp(-n\epsilon/p) \\ &= \exp\left[-\int_{-\infty}^{\infty} d\omega J(p,\omega,t) \right. \\ &\quad \left. + \int_{-\infty}^{\infty} d\omega J(p+\omega,\omega,t)e^{-\omega/(p/n)}\right]. \end{aligned} \tag{8}$$

For this to be approximately constant, or at least have a weak dependence on p, the exponent

$$A(p,t,n) = -\int_{-\infty}^{\infty} d\omega J(p,\omega,t) + \int_{-\infty}^{\infty} d\omega J(p+\omega,\omega,t)e^{-\omega/(p/n)} \tag{9}$$

must have weak dependence on p, at most equaling $\beta \ln p$ with $\beta < 1$.

Even without knowing the explicit form of the J function, some insight can be gained from this expression. First, for the second integral to be well defined in the $\omega < 0$ range, the Boltzmann factor corresponding to the thermal partons must compensate the $e^{-\omega/(p/n)}$ factor. Second, because of the $e^{-\omega/(p/n)}$ factor, in general the loss term dominates and hence

$R_{AA}(p) < 1$. Third, as $p \to \infty$, the compensation between the two terms in A becomes complete and $R_{AA} \to 1$.

To be more specific, the precise form of the J function needs to be known. The energy loss of an energetic parton in a dense medium mainly proceeds via bremsstrahlung of soft gluons. The form of the energy loss (the J function above) depends crucially on whether bremsstrahlung off many scatterers are coherent or incoherent. This is determined by the relative size of the mean free path $\lambda = 1/n\sigma$ and the coherence length [24],

$$l_{\rm coh} = \sqrt{\frac{\lambda\omega}{\mu^2}} \tag{10}$$

where μ is the typical size of the soft momentum exchange and ω is the energy of the emitted gluon. When $l_{\rm coh} \ll \lambda$, then one is in the extreme Bethe-Heitler regime where the energy loss per unit length is proportional to the incoming energy. Conversely, when $l_{\rm coh} \gg \lambda$, then one is in the extreme Landau-Pomeranchuk-Migdal (LPM) regime where the energy loss per unit length is proportional to the square-root of the incoming energy.

The typical mean free path for soft scattering in a hot medium can be estimated as follows. The density of scatterers according to the thermal distribution is $n \sim T^3$. The typical soft ($p_{\rm exch} \sim gT$) scattering cross-section is given by $\sigma \sim g^2/T^2$. Hence

$$\lambda \sim 1/g^2 T. \tag{11}$$

According to the above estimate of the coherence length, the LPM effect becomes relevant when $l_{\rm coh} \gtrsim \lambda$ or

$$\frac{\omega}{\mu^2} \gtrsim \lambda, \tag{12}$$

with $\mu \sim gT$ and $\lambda \sim 1/g^2 T$. This yields the following condition:

$$\omega \gtrsim T. \tag{13}$$

Defining $E_{\rm LPM} = \lambda\mu^2$, one can then conclude that for the emitted gluon energy in the range of $0 < \omega < E_{\rm LPM}$, energy loss is governed by the Bethe-Heitler limit as follows:

$$\omega \frac{dI}{d\omega dz} \simeq \frac{\alpha_s}{\pi} N_c \frac{1}{\lambda}, \tag{14}$$

and for $\omega > E_{\rm LPM}$, the energy loss is governed by the LPM limit [24] as follows:

$$\omega \frac{dI}{d\omega dz} \simeq \frac{\alpha_s}{\pi} N_c \sqrt{\frac{\mu^2}{\lambda\omega}}. \tag{15}$$

For $\omega > E_{\rm LPM}(L/\lambda)^2$, the coherence length exceeds the length of the medium. In this case, effectively only a single scattering can occur and the radiation spectrum goes back to

$$\omega \frac{dI}{d\omega dz} \simeq \frac{\alpha_s}{\pi} N_c \frac{1}{L}. \tag{16}$$

In this article, we will consider only following the case:

$$0 < E_{\rm LPM} \leqslant E_0 < E_{\rm fact} \tag{17}$$

assuming that $L/\lambda \gg 1$. Here E_0 denotes the original energy of the parton and we defined $E_{\rm fact} = E_{\rm LPM}(L/\lambda)^2$.

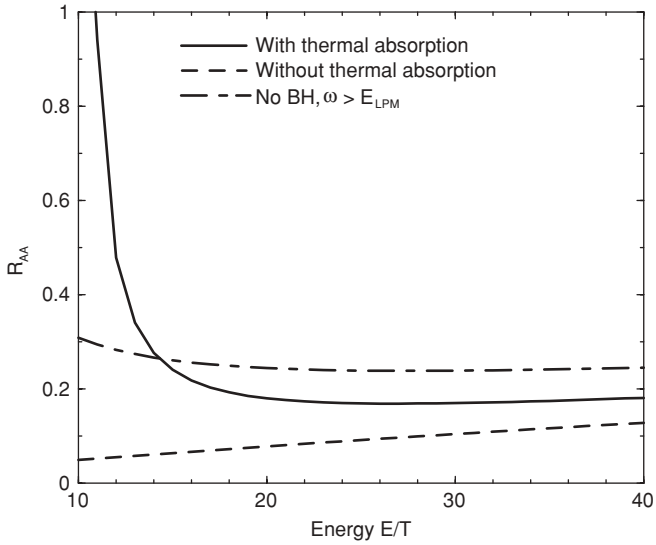

FIG. 2. Approximate $R_{AA}(p)$ calculated with Eq. (9) following the approach of BDMPS up to the maximum momentum of $E_{\rm fact} = 16\,{\rm GeV}$. The solid line includes the contribution from absorption of thermal gluons whereas the broken line only includes the emission. The dashed-dotted line is calculated with only the LPM part of the gluon spectrum. The divergence at $p = 10T$ is an artifact of the approximation.

To use Eq. (9), in addition to the above forms of gluon spectrum for $\omega > 0$, we also need to know the form of $J(p, \omega, t)$ for $\omega < 0$. For simplicity, we take the spectrum for $\omega < 0$ to be the same as the Bethe-Heitler spectrum and multiply it by the Boltzmann factor to take into account that absorption of high energy gluons from the thermal medium is Boltzmann suppressed:

$$\frac{dI}{d\omega dz} = \frac{\alpha_s N_c}{\pi\lambda} \frac{1}{|\omega|} e^{-|\omega|/T}. \tag{18}$$

For illustration, we set $E_{\rm LPM} = 1\,{\rm GeV}$, $\lambda = 1$ fm and $T = 400\,{\rm MeV}$ and evolve the system until $L = ct = 4$ fm. We have also set the upper limit of the momentum integral to p. The above simple gluon spectrum then yields the $R_{AA}(p)$ curves shown in Figs. 2 and 3. The solid curves in the figures are calculated including the absorption contribution, and the broken curves are calculated without the absorption part. Also shown are the dot-dashed curves, which are calculated with only the $\omega > E_{\rm LPM}$ part of the gluon spectrum, omitting the Bethe-Heitler part. In Fig. 3, we show a momentum range far exceeding the factorization energy to compare with the calculation in Ref. [23].

In Ref. [23], two of us have calculated the same ratio of the final and the initial spectrum using the resummation method developed by AMY. The shape and the trend of the curve calculated with the thermal absorption in Figs. 2 and 3 closely match up with what we have previously calculated in Ref. [23]. The experimentally obtained R_{AA} from STAR and PHENIX from RHIC experiments also roughly has the same shape and trend [2,25].

There are two major points we would like to make with this simple calculation. One is the importance of the *absorption*

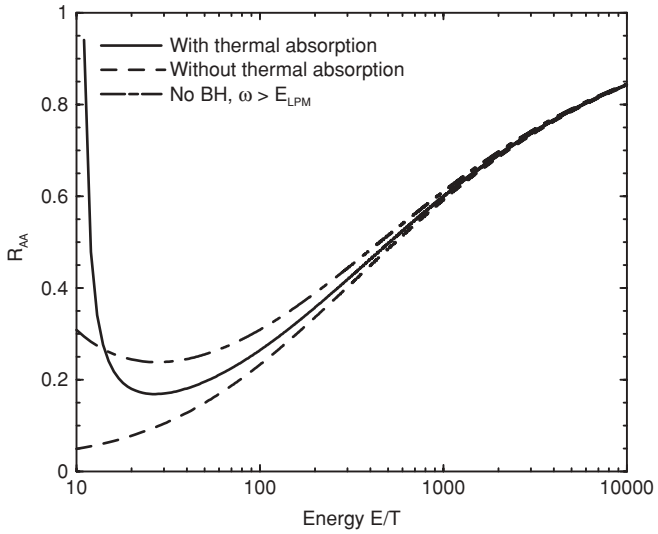

FIG. 3. The same as Fig. 2 but showing a larger energy range.

of the thermal gluons. This is also closely related to the appearance of a momentum scale $p = nT$. Near this scale, absorption of thermal gluons is very efficient in changing the shape of the final spectrum. Comparing the two curves in Fig. 2 and also in Fig. 3, it is clear that the roughly flat shape within the limited momentum range shown in Fig. 2 is because of the absorption of thermal gluons. Furthermore, the efficient absorption near $p = nT$ causes R_{AA} to have a larger value near this point. Without the absorption, R_{AA} is a monotonically increasing function of p. In the experimentally measured R_{AA}, one does observe such a change in slope near $p_T = 3\,\text{GeV}$. This is usually attributed to the Cronin effect. However, it could very well be because of the absorption of thermal gluons.

The importance of gluon absorption will arise whenever the slope of the spectrum, $d \ln P/dp$, is comparable with the thermal value $1/T$. When these are equal, detailed balance ensures that the more numerous lower energy particles keep repopulating the higher energy ones. The reason the spectrum in Fig. 2 rises to 1 at $10T$ is because we took the initial particle distribution to be a strict power law, $\sim p^{-n}$, which becomes steeper than the thermal spectrum below $p = nT$. More realistic initial distributions, as in Eq. (2), will not display this behavior; nevertheless, absorption is important in the lower energy region.

Another point to make is the importance of the Bethe-Heitler part of the radiation spectrum. The effect of neglecting the Bethe-Heitler part of the spectrum becomes justifiable only around $p \sim 100T$. Therefore, calculations with only the LPM part of the spectrum appear unrealistic for RHIC energies.

III. THE FORMALISM

In a seminal series of articles, Baier, Dokshitzer, Mueller, Peigné, and Schiff identified the diagrams that contribute to the leading order energy loss in a hot QGP medium. A typical diagram is shown in Fig. 4. To compute the energy loss rate, one must deal with the following issues:

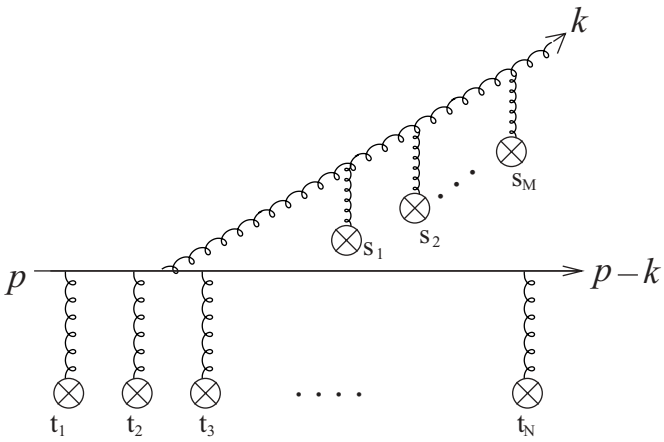

FIG. 4. A typical bremsstrahlung diagram that needs to be resummed.

1. How are these diagrams to be resummed?
2. How is the resulting equation to be solved?
3. How does one describe the *time evolution* of the energy loss?

We now summarize the approach taken by AMY. The ingredients discussed in this section can be found in Ref. [23]. We also briefly compare it with other approaches.

In the diagram shown in Fig. 4, a single wiggly line connected to a single $\otimes$ is not a gluon propagator. Rather, it just denotes that a quark has interacted with the soft background field at a certain time t_i or s_i. To get the gluon energy spectrum at the final time, we need to sum all the diagrams of the type shown in Fig. 4, then square and average over the soft field configurations. This procedure leads to the conclusion that the scattering rate can be obtained by calculating the imaginary part of the gluon self-energy in the soft thermal background. A typical gluon self-energy in such a situation is shown in Fig. 5.

The result of resummation is summarized in the following formulas. The transition rates for various emission processes are given by the following:

$$\frac{d\Gamma(p,k)}{dkdt} = \frac{C_s g_s^2}{16\pi p^7} \frac{1}{1 \pm e^{-k/T}} \frac{1}{1 \pm e^{-(p-k)/T}} \times \begin{Bmatrix} \frac{1+(1-x)^2}{x^3(1-x)^2} & q \to qg \\ N_f \frac{x^2+(1-x)^2}{x^2(1-x)^2} & g \to qq \\ \frac{1+x^4+(1-x)^4}{x^3(1-x)^3} & g \to gg \end{Bmatrix} \times \int \frac{d^2\mathbf{h}}{(2\pi)^2} 2\mathbf{h} \cdot \text{Re}\,\mathbf{F}(\mathbf{h}, p, k). \quad (19)$$

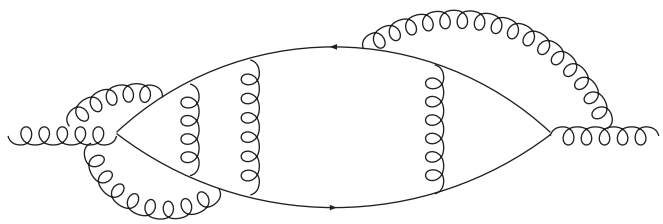

FIG. 5. A typical gluon self-energy diagram that needs to be resummed.

Here C_s is the quadratic Casimir relevant for the process (in QCD, 4/3 for processes involving a quark and 3 for the pure glue process) and $x \equiv k/p$ is the momentum fraction in the gluon (or the quark, for the case $g \to q\bar{q}$). The factors $1/(1 \pm e^{-k/T})$ are Bose stimulation or Pauli blocking factors for the final states, with $-$ for bosons and $+$ for fermions. $\mathbf{h} \equiv \mathbf{p} \times \mathbf{k}$ determines how noncollinear the final state is; we treat it as parametrically $O(gT^2)$ and therefore small compared to $\mathbf{p} \cdot \mathbf{k}$. Therefore it can be taken as a two-dimensional vector in the transverse space. $\mathbf{F}(\mathbf{h}, p, k)$ is the solution of the following integral equation:

$$\begin{aligned} 2\mathbf{h} = {} & i\delta E(\mathbf{h}, p, k)\mathbf{F}(\mathbf{h}) + g_s^2 \int \frac{d^2\mathbf{q}_\perp}{(2\pi)^2} C(\mathbf{q}_\perp) \\ & \times \big\{(C_s - C_A/2)[\mathbf{F}(\mathbf{h}) - \mathbf{F}(\mathbf{h} - k\,\mathbf{q}_\perp)] \\ & + (C_A/2)[\mathbf{F}(\mathbf{h}) - \mathbf{F}(\mathbf{h} + p\,\mathbf{q}_\perp)] \\ & + (C_A/2)[\mathbf{F}(\mathbf{h}) - \mathbf{F}(\mathbf{h} - (p-k)\,\mathbf{q}_\perp)]\big\}. \end{aligned} \tag{20}$$

Here $C(\mathbf{q}_\perp)$ is the differential rate to exchange transverse (to the parton) momentum $\mathbf{q}_\perp$. In a hot thermal medium, its value at leading order in α_s is [26] as follows:

$$C(\mathbf{q}_\perp) = \frac{m_D^2}{\mathbf{q}_\perp^2(\mathbf{q}_\perp^2 + m_D^2)}, \quad m_D^2 = \frac{g_s^2 T^2}{6}(2N_c + N_f). \tag{21}$$

The energy difference between the final and the initial states is given by the following:

$$\delta E(\mathbf{h}, p, k) = \frac{\mathbf{h}^2}{2pk(p-k)} + \frac{m_k^2}{2k} + \frac{m_{p-k}^2}{2(p-k)} - \frac{m_p^2}{2p}, \tag{22}$$

where m^2 are the medium induced thermal masses, equal to $m_D^2/2$ for a gluon and $C_f g_s^2 T^2/4 = g_s^2 T^2/3$ for a quark. For the case of $g \to qq$, $(C_s - C_A/2)$ should appear as the prefactor on the term containing $\mathbf{F}(\mathbf{h} - p\,\mathbf{q}_\perp)$ rather than $\mathbf{F}(\mathbf{h} - k\,\mathbf{q}_\perp)$.

Next, we use these expressions to evolve the hard gluon distribution $P_g(p, t = 0)$ and the hard quark plus antiquark distribution $P_{q\bar{q}}(p, t = 0)$ with time, as they traverse the medium. The joint equations for $P_{q\bar{q}}$ and P_g are

$$\begin{aligned} \frac{dP_{q\bar{q}}(p)}{dt} &= \int_k P_{q\bar{q}}(p+k)\frac{d\Gamma_{qg}^q(p+k,k)}{dkdt} - P_{q\bar{q}}(p)\frac{d\Gamma_{qg}^q(p,k)}{dkdt} + 2P_g(p+k)\frac{d\Gamma_{q\bar{q}}^g(p+k,k)}{dkdt}, \\ \frac{dP_g(p)}{dt} &= \int_k P_{q\bar{q}}(p+k)\frac{d\Gamma_{qg}^q(p+k,p)}{dkdt} + P_g(p+k)\frac{d\Gamma_{gg}^g(p+k,k)}{dkdt} - P_g(p)\left(\frac{d\Gamma_{q\bar{q}}^g(p,k)}{dkdt} + \frac{d\Gamma_{gg}^g(p,k)}{dkdt}\Theta(2k-p)\right), \end{aligned} \tag{23}$$

where the k integrals run from $-\infty$ to ∞. The integration range with $k < 0$ represents absorption of thermal gluons from the QGP; the range with $k > p$ represents annihilation against an antiquark from the QGP, of energy $(k - p)$. In writing Eq. (23), we used $d\Gamma_{gg}^g(p,k) = d\Gamma_{gg}^g(p, p-k)$ and similarly for $g \to q\bar{q}$; the Θ function in the loss term for $g \to gg$ prevents double counting of final states. Because bremsstrahlung energy loss involves only small $O(g_s T/p)$ changes to the directions of particles, these equations can be used for the momentum distributions in any particular direction. For a single initial hard particle, they can be viewed as Fokker-Planck equations for the evolution of the probability distribution of the particle energy and of accompanying gluons. These expressions depend at several points on g_s^2 or α_s. When evaluating them numerically, we have used $\alpha_s = 0.3$.

We now briefly compare our approach with others used in the literature. As this article is not intended to be a review, this cannot and will not be a complete comparison with all other jet-energy loss calculations.

As was mentioned at the beginning of this section, most jet-quenching calculations start with the problem of resumming all diagrams of the form shown in Fig. 4. In a series of articles, U. Wiedemann *et al.* have shown that BDMPS, Zakharov, GLV, and also the eikonal approach taken by Wiedemann and Kovner are all related to each other. In these approaches, the problem of resumming the diagrams is solved in position space assuming *static scatterers*, although the methods of solving the problem differ. Because a thermal medium consists of dynamic, moving scatterers, temperature was introduced only as the controlling variable for the mean free path in these approaches. The evolution of the initial parton distribution is then achieved through Eq. (4) with the important restrictions that only the *emission* of gluons was considered with (Wiedemann) or without (BDMPS) restriction on the kinematic upper limit of the emitted energy. There is also an approximation that ignores the emitted energy in the gain rate $[\Gamma(p + \omega, \omega, t) \to \Gamma(p, \omega, t)$ in Eq. (4)].

Our approach differs with the above ones in three major ways. The biggest difference is that our calculation is completely thermal and hence the scatterers are all dynamic. In our calculation, temperature enters through the thermal phase space of the initial and the final particles and there is no assumption of the form of the elementary cross section. All are calculated completely within the framework of hard thermal loop resummed leading order thermal QCD. Hence, gain or loss because of the absorption of thermal partons ($\omega < 0$) as well as the loss process of pair annihilations with the thermal partons ($\omega > p$) are fully included in our calculation. These are missing in the approaches mentioned above. In Ref. [27], thermal absorption and stimulated emission were introduced

in the framework of GLV. This was done only up to the first order in the opacity expansion without including the annihilation process with thermal partons. Second, instead of approximately solving for the transition rates and then using Eq. (4), we explicitly solve for both the transition rates and the coupled rate equations of hard quarks and gluons. There are also no approximations about whether the Bethe-Heitler or LPM regime is relevant; the transition between these extremes is handled correctly.

One limitation of the current approach as compared to the previous ones is that the transition rates are calculated in momentum space assuming the thermodynamic limit. That is, our approach assumes that the high-energy parton experiences a uniform medium on the time scale of the formation time of the emitted radiation. Hence, our approach is limited to momenta less than the factorization energy. With $\mu \approx 0.5$ GeV, $L \approx 5$ fm, and $\lambda \approx 1$ GeV, this limits the momenta to the region $p < 30$ GeV. This is not a big problem at RHIC energies, where $\sqrt{s}$ is only 200 GeV, and it also covers the p_T acceptance of the ALICE detector at the LHC.

IV. PION PRODUCTION

The goal of this section is to use the formalism explained in the previous section to calculate the neutral pion spectrum in heavy-ion collisions. Our approach to this problem relies on the fact that for hard spectra, the *AA* collision can be regarded as a collection of binary collisions. In this way of formulating the problem, the *AA* spectrum is given by the convolution of the elementary *pp* spectrum with geometrical and in-medium factors.

Up to suppressed corrections, the π^0 cross section in an *N-N* collision factorizes and is given by [28] the following:

$$E_\pi \frac{d\sigma_{NN}}{d^3p_\pi} = \sum_{a,b,c,d} \int dx_a dx_b g(x_a, Q) g(x_b, Q) K_{\text{jet}} \times \frac{d\sigma^{a+b\to c+d}}{dt} \frac{1}{\pi z} D_{\pi^0/c}(z, Q'), \quad (24)$$

where $g(x, Q)$ is the parton distribution function (PDF) in a nucleon, $D_{\pi^0/c}(z, Q')$ is the pion fragmentation function, $d\sigma^{a+b\to c+d}/dt$ is the parton-parton cross-section at leading order, and the factor K_{jet} accounts for higher order effects (where jet here means a fast parton having $p_T^{\text{jet}} \gg 1$ GeV). According to [29], K_{jet} is almost independent of p_T^{jet} at RHIC energies. We use $K_{\text{jet}} \sim 1.7$ for RHIC and 1.6 for the LHC, based on their results.

For all our calculations, we set the factorization scale (Q) and the fragmentation scale (Q') equal to p_T. We take the CTEQ5 parton distribution function [30] and the π fragmentation function extracted from e^+e^- collisions [31].

Figure 6 shows our calculation for the spectrum of high p_T neutral pions in *pp* collisions at RHIC, compared to the PHENIX result [32]. One can readily see that our calculation reproduces the data in the region where jet fragmentation is expected to be the dominant mechanism of particle production ($p_T > 5$ GeV/c) [33].

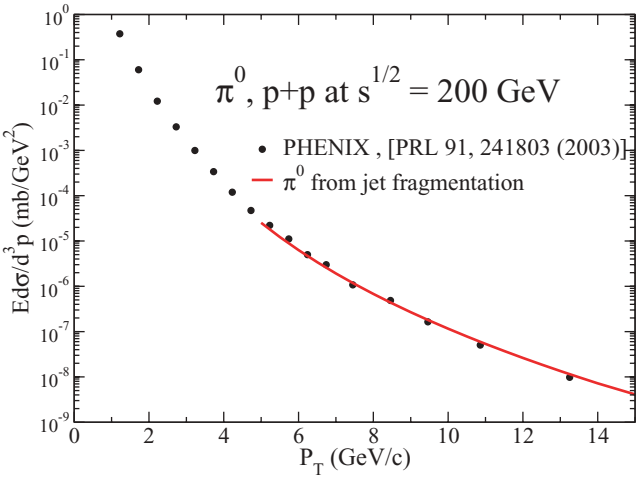

FIG. 6. (Color online) Neutral pion spectra in *pp* collisions at RHIC. The data points are from PHENIX and the solid line is the calculated result from jet fragmentation.

To obtain the high p_T π^0 cross-section in *AA* collisions, we must modify the *pp* calculation in two ways. First, the PDF of a nucleus differs from that of a proton as follows:

$$g_A(x_a, Q) = g(x_a, Q) R_A(x_a, Q), \quad (25)$$

where the nuclear modification of the structure function R_A takes into account shadowing and antishadowing. In this article, we use $R_A(x_a, Q)$ as parametrized by Eskola *et al.* [34].

Second, we must account for the energy loss of the parton between its production in the hard initial scattering event and its hadronization. We assume that a jet fragments only outside the medium, as may be justified by estimating the formation time of a pion with the typical observed energy. In Ref. [35], the formation time of an emitted pion with energy E_π is estimated to be $\sim R_\pi E_\pi / m_\pi$, where $R_\pi \sim 1$ fm is the size of the pion. For a 10-GeV pion, this gives $\tau_f \sim 35$–70 fm/c. This is much longer than the path of a jet in the hot matter created by two colliding nuclei. Therefore, one should consider production, energy loss in medium, and fragmentation to occur sequentially.

We assume that the fragmentation at the edge of the QGP involves the usual vacuum fragmentation function. The medium effect is then to reduce the parton energy by an amount determined by the Fokker-Planck equation previously presented, Eq. (23). This is most conveniently written by defining a new medium-inclusive effective fragmentation function,

$$\tilde{D}_{\pi^0,c}(z, Q; \mathbf{r}, \mathbf{n}) = \int dp_f \frac{z'}{z} [P_{q\bar{q}/c}(p_f; p_i) D_{\pi^0/q}(z', Q) + P_{g/c}(p_f; p_i) D_{\pi^0/g}(z', Q)], \quad (26)$$

where $z = p_T/p_i$ and $z' = p_T/p_f$. $P_{q\bar{q}/c}(p_f; p_i)$ and $P_{g/c}(p_f; p_i)$ represent the solution to Eq. (23), which is the probability to get a given parton with final momentum p_f when the initial condition is a particle of type c and momentum p_i.

The quantities $P_{q\bar{q}/c}$ and $P_{g/c}$ in Eq. (26) depend implicitly on the path length the initial parton must travel and the

temperature profile along that path. This is not the same for all jets, because it depends on the location where the jet is produced and on the direction the jet propagates. Therefore, one must convolve this expression over all transverse positions $\mathbf{r}_\perp$ and directions $\mathbf{n}$. Because the number of jets at $\mathbf{r}_\perp$ is proportional to number of binary collisions, the probability is proportional to the product of the thickness functions of the colliding nuclei at $\mathbf{r}_\perp$. For central collisions where the impact parameter $b \approx 0$, we get the following:

$$\mathcal{P}(\mathbf{r}_\perp) \propto T_A(\mathbf{r}_\perp) T_B(\mathbf{r}_\perp). \tag{27}$$

For a hard sphere that we use for simplicity, this probability is as follows:

$$\mathcal{P}(\mathbf{r}_\perp) = \frac{2}{\pi R_\perp^2}\left(1 - \frac{r_\perp^2}{R_\perp^2}\right)\theta(R_\perp - r_\perp), \tag{28}$$

which is normalized to yield $\int d^2 r_\perp \mathcal{P}(\mathbf{r}_\perp) = 1$. Because the direction of the jet is fixed by the pion direction ($\mathbf{n} = \mathbf{p}_\pi/|\mathbf{p}_\pi|$), the final in-medium modified fragmentation function is as follows:

$$\tilde{D}_{\pi^0/c}(z, Q) = \int d^2 r_\perp \, \mathcal{P}(\mathbf{r}_\perp) \tilde{D}_{\pi^0/c}(z, Q, \mathbf{r}_\perp, \mathbf{n}). \tag{29}$$

The AA spectrum is now given by the following:

$$\frac{dN_{AA}}{dy d^2 p_T} = \frac{\langle N_{\rm coll}\rangle}{\sigma_{\rm in}} \sum_{a,b,c,d} \int dx_a dx_b g_A(x_a, Q) g_A(x_b, Q) K_{\rm jet} \times \frac{d\sigma^{a+b\to c+d}}{dt} \frac{\tilde{D}_{\pi^0/c}(z, Q)}{\pi z}, \tag{30}$$

where $\langle N_{\rm coll}\rangle$ is the average number of binary collisions and $\sigma_{\rm in}$ is the inelastic nucleon-nucleon cross section.

Because Eq. (30) is expressed in terms of probability distributions, it is straightforward to evaluate it using the Monte Carlo method. One complication in doing so is that, although the parton traverses the medium, the medium also evolves. Therefore at each time step of solving Eq. (23), the temperature must be adjusted to the local environment. We assume that the medium expands only in the longitudinal direction, based on the following reasoning. The low p_T neutral pion spectrum at RHIC is well reproduced by a hydrodynamical model incorporating transverse expansion, whereas the model fails for $p_T > 3$ GeV, suggesting that high-p_T pions mainly come from jet fragmentation [36]. The transverse expansion will have two effects on jet energy loss. First, the expanding geometry will increase the duration of parton propagation. However, the same expansion will cause the parton density to fall along the path. Those two effects partially compensate each other and the energy loss is just about the same as in the case without transverse expansion [37]. In 1D Bjorken expansion [38], the temperature evolves as follows:

$$T = T_i \left(\frac{\tau_i}{\tau}\right)^{1/3}. \tag{31}$$

In the original Bjorken model, the transverse density is assumed to be constant. Because a nucleus does have a transverse density profile, it is more realistic to assign the initial temperatures in the transverse direction according to the local density so that [39,40]

$$T(r, \tau_i) = T_i \left[2\left(1 - \frac{r^2}{R_\perp^2}\right)\right]^{1/4}. \tag{32}$$

Putting Eqs. (31) and (32) together, we get the temperature evolution of a QGP expanding in 1D as follows:

$$T(r, \tau) = T_i \left(\frac{\tau_i}{\tau}\right)^{1/3} \left[2\left(1 - \frac{r^2}{R_\perp^2}\right)\right]^{1/4}. \tag{33}$$

The jet evolves in the QGP medium until it reaches the surface or until the temperature reaches the transition temperature T_c. In our calculation, we assume a first-order phase transition and use the following:

$$f_{\rm QGP} = \frac{1}{r_d - 1}\left(\frac{r_d \tau_f}{\tau} - 1\right) \tag{34}$$

as the fraction of the QGP phase in the mixed phase [38]. Here $r_d = g_Q/g_H$ is the ratio of the degrees of freedom in the two phases and τ_f is the time when the temperature reaches T_c. The evolution equation is then scaled accordingly for $\tau > \tau_f$. We take the critical temperature T_c to be 160 MeV.

The result of our calculation for RHIC energy is summarized in Fig. 7 together with the PHENIX data [2]. To cover the uncertainties in the initial conditions, we consider two different sets, one at a relatively high temperature of $T_i = 447$ MeV and a relatively short initial time of $\tau_i = 0.147\,{\rm fm}/c$ taken from Refs. [39,40], and one at a lower temperature $T_i = 370$ MeV and somewhat later time for the hydrodynamic evolution of $\tau_i = 0.26\,{\rm fm}/c$ taken from Ref. [41]. Those two sets correspond to $dN/dy|_{y=0} \sim 1260$, estimated for central collisions in Ref. [40]. In deriving these results, we have used $\alpha_s = 0.3$. If the value is larger then energy loss will be greater, so R_{AA} will be smaller; if it is

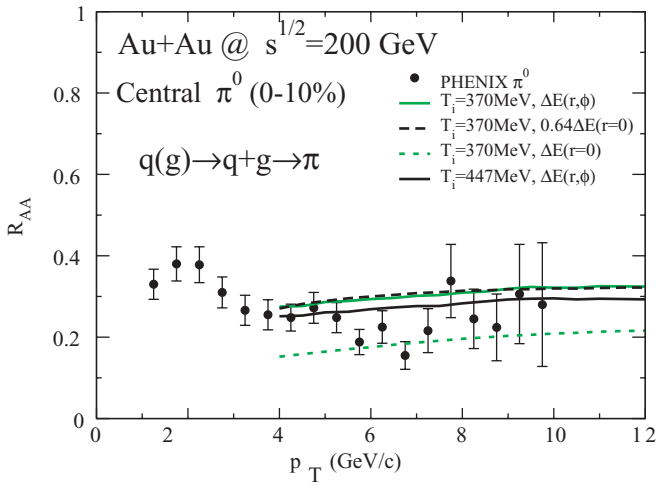

FIG. 7. (Color online) Nuclear modification factor for pions at RHIC. Data points are from PHENIX [2]. The solid lines show the full calculation of the spatial distribution of jets in the transverse plane for two initial temperatures. The dotted lines assume that all jets are created at the center and the dashed lines assume the same approximation but with a reduced energy loss.

smaller, then R_{AA} increases. Besides this dependence on α_s, our results rely on no free parameters.

The solid lines in the figure are full calculations with the initial spatial distribution $\mathcal{P}(\mathbf{r}_\perp)$ given in Eq. (28). For comparison, we also display two more sets of calculations. The dotted line is calculated with the jets originating only from the center of the disk ($\mathbf{r}_\perp = 0$). Comparing the dotted line with the solid line, it is apparent that the absolute magnitude of the R_{AA} depends very much on the density profile of the nucleus. The dashed line is calculated again with the jets from the center but with the energy loss rates reduced by a factor of 0.64. One may say that the average path of a jet has the length of about $0.64 \times R_A$.

In Fig. 7, one can see that both $T_i = 447\,\mathrm{MeV}$ and $T_i = 370\,\mathrm{MeV}$ describe the real data reasonably well. This is somewhat surprising. Because the density of thermal particle is proportional to T^3, the density at 447 MeV is about 1.8 times the density at 370 MeV. Yet the energy loss does not reflect such a big difference. The reason is because the energy loss depends mostly on the duration of evolution. In a Bjorken expansion, the initial time τ_i and the temperature are related by the following:

$$T_i^3 \tau_i = \frac{\pi^2}{\zeta(3) g_Q} \frac{1}{\pi R_\perp^2} \frac{dN}{dy}. \tag{35}$$

Hence once dN/dy is fixed, the time evolution of the temperature follows a common curve regardless of the initial temperature [cf., Eq. (33)]. The only difference between the higher and the lower temperature cases is that the time evolution starts earlier for the higher temperature case. From the moment τ passes τ_i for the lower temperature, the evolution of the two systems is identical. Therefore, if energy loss at the beginning of the evolution is small compared to the later time energy loss, the amount of energy loss depends mostly on the duration of the QGP phase $\Delta\tau = \tau_f - \tau_i$. Because $\tau_f \gg \tau_i$, the duration of the QGP phase is approximately the same for high temperatures. We have verified that the energy loss between the times corresponding to $T_i = 1000\,\mathrm{MeV}$, $T_i = 447\,\mathrm{MeV}$, and $T_i = 370\,\mathrm{MeV}$ are at most about 10%.

Because the suppression is mainly controlled by the duration of the evolution, the suppression should be sensitive to the particle rapidity density dN/dy, which fixes the lifetime of the QGP. We can see in Fig. 8 that it is indeed the case. For simplicity, we assume here that the jets are all created at the center of the system. We see that there is very little change in the suppression as the initial temperature varies from $T_i = 370$ MeV to $T_i = 1000$ MeV. However, the suppression shows a strong dependence on dN/dy; going from $dN/dy = 680$ to $dN/dy = 1260$ increases the suppression by a factor of $\sim$1.5.

For the LHC, we use the initial temperature from Ref. [41], $T_i = 845$ MeV, giving $\tau_i = 0.088$ fm/c for $dN/dy \sim 5625$ [40,42]. At this energy, jets could in principle be produced with energies as high as $\sqrt{s}/2 = 2750$ GeV. However, according to our discussion in Sec. II, the contribution from a jet having more that twice the observed pion energy should be sharply cut off by the steeply falling initial function. Because our approach is limited to the observed $p_T \gtrsim 30$ GeV, considering original energy of only up to about 100 GeV should be enough for our purposes. To be on the conservative side, we cut off the maximum jet energy at 400 GeV.

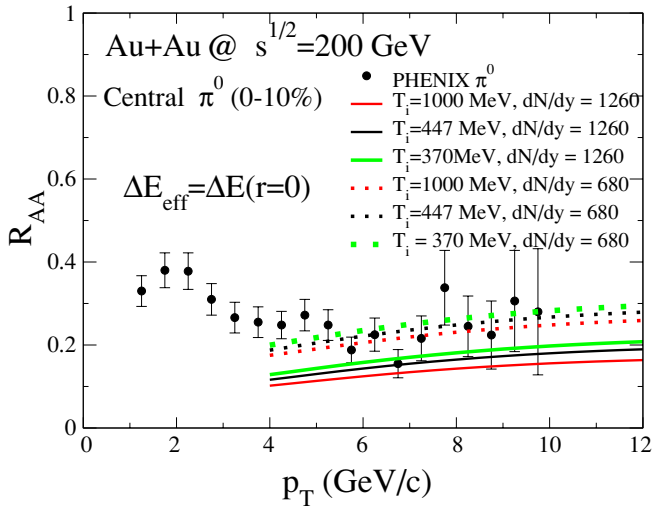

FIG. 8. (Color online) Nuclear modification factor for pions at RHIC, taking all jets to originate at the center of the nucleus. Data points are from PHENIX [2]. The solid lines are for initial conditions which lead to a particle multiplicity of $dN/dy = 1260$, whereas the dotted lines are for initial conditions leading to $dN/dy = 680$. For each set of lines, the initial temperature is, from bottom to top, 1000, 447, and 370 MeV.

The calculated LHC nuclear modification factor is shown in Fig. 9 with the full fragmentation function from Eq. (29). We also show in the same figure the effect of not tracking the secondary partons (gluons emitted by quarks and quarks emitted by gluons). Comparison between the solid line and the dashed line shows that ignoring the secondaries can make an overall difference of 30%. This arises almost entirely from

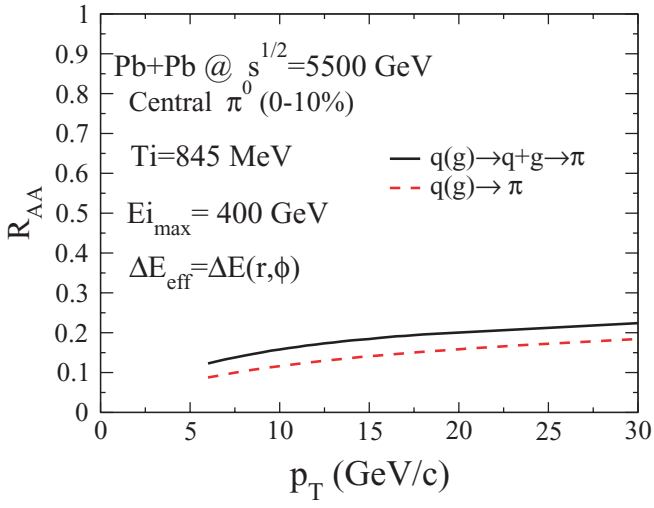

FIG. 9. (Color online) Nuclear modification factor of pions at the LHC. The solid line includes pions coming from bremsstrahlung secondaries emitted in the thermal medium; the dashed line does not. For both lines, the full spatial distribution from Eq. (28) has been used.

quark secondaries from gluon jets—that is, from hard gluons that split, due to plasma interactions, into $q\bar{q}$ pairs, which subsequently fragment. This is important at the LHC, but much less so at RHIC, because most hard jets at the LHC arise from gluons, whereas a larger fraction at RHIC are from quarks. The gluons emitted by quarks are mostly soft; they also lose energy quickly and fragment inefficiently. At RHIC energies the error from dropping secondaries is only 5%.

Comparing the RHIC and LHC results, we see that the suppression because of jet energy loss at RHIC is about a factor of 3 for a 10 GeV pion, whereas the suppression at the LHC for a pion at the same energy is about a factor of 6. This difference arises because the medium at the LHC remains hot for much longer than at RHIC. The cooling is governed by the product $T^3\tau \propto dN/dy$. Hence, smaller dN/dy implies faster cooling. We have also calculated the impact of assuming a first-order phase transition. At RHIC, at the end of the QGP phase, many jets have already left the medium, but those still inside will suffer additional suppression during the mixed phase, such that assuming a crossover between the QGP and the hadron gas phase will increase R_{AA} by ∼20%. At the LHC, at the critical point, a much larger fraction of jets are out of the medium, such that R_{AA} is quite insensitive to assumptions related to the transition. Our initial conditions correspond to an initial time smaller than the common value of $\tau_i = 0.6$ fm/c used in hydrodynamic calculations [43]. We have verified that going from $\tau_i = 0.26$ fm/c ($T_i = 370$ MeV) to 0.6 fm/c ($T_i = 280$ MeV) increases R_{AA} by less than 20%. In this section, the AMY formalism has been applied to successfully reproduce the π^0 spectra at RHIC. We will see in the following section how the same formalism can be applied to determine the production of real photons.

V. PHOTON PRODUCTION

The hard photons produced in nucleon-nucleon collisions can be divided into three categories: direct photons, fragmentation photons, and background photons. Direct photons are those produced by Compton scattering and annihilation of two incoming partons. Fragmentation photons are those produced by bremsstrahlung emitted from final state partons. Background photons are those produced by the decay of hadrons subsequent to the collision, primarily from $\pi^0 \to \gamma\gamma$ decay. The "prompt photons" are those coming from direct production and the fragmentation process. The expression for prompt photon production is

$$E_\gamma \frac{d\sigma}{d^3p_\gamma} = \sum_{a,b} \int dx_a dx_b g(x_a, Q) g(x_b, Q) \times \left\{ K_\gamma(p_T) \frac{d\sigma^{a+b\to\gamma+d}}{dt} \frac{2x_a x_b}{\pi\left(2x_a - 2\frac{p_T}{\sqrt{s}}e^y\right)} \times \delta\left(x_b - \frac{x_a p_T e^{-y}}{x_a\sqrt{s} - p_T e^y}\right) + K_{\rm brem}(p_T) \frac{d\sigma^{a+b\to c+d}}{dt} \frac{1}{\pi z} D_{\gamma/c}(z, Q) \right\}. \quad (36)$$

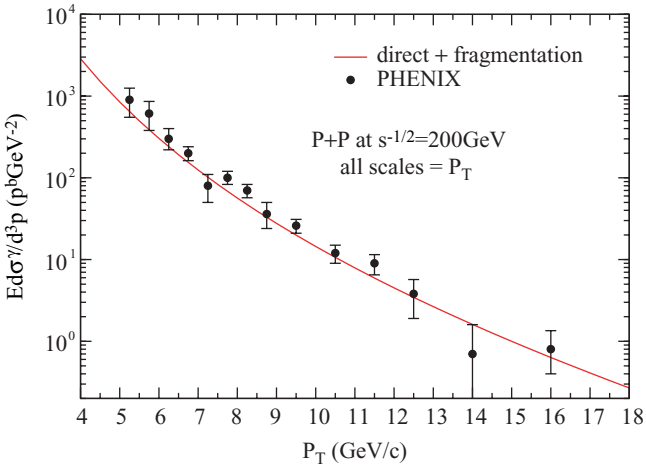

FIG. 10. (Color online) Prompt photons produced in pp collision at RHIC. Data points are from PHENIX. The solid line is calculated with Eq. (36).

K_γ and $K_{\rm brem}$ are correction factors to take into account NLO effects; we evaluate them using the numerical program from Aurenche *et al.* [44], obtaining $K_\gamma(10\ {\rm GeV}) \sim 1.5$ for RHIC and LHC and $K_{\rm brem}(10\ {\rm GeV}) \sim 1.8$ at RHIC and 1.4 at LHC. All scales (renormalization, factorization, and fragmentation) have been set equal to the photon transverse momentum p_T. The photon fragmentation function $D_{\gamma/c}$ is extracted without medium effects in $e^- + e^+$ collisions [45]. The validity of this expression for pp collisions at $\sqrt{s} = 200$ GeV is shown in Fig. 10 with data from PHENIX [46]. It appears clear that the baseline mechanism of high p_T photon production in nucleon-nucleon collisions is under quantitative control.

In AA collisions, there is an additional source of high p_T photons: the medium contribution. This contribution includes the direct conversion of a high-energy parton to a high-energy photon by annihilation with a thermal parton, in-medium bremsstrahlung from a jet, and thermal production of photons.

A. Jet-photon conversion

In Ref. [39], the conversion of a leading parton to a photon in the plasma was found to be an important process. This happens when a jet crossing the hot medium undergoes an annihilation ($q + \bar{q} \to g + \gamma$) or a Compton ($g + q \to q + \gamma$) process with a thermal parton. The related production rate of photons is given by [39,47] the following:

$$\frac{dR}{dy d^2p_T} = \sum_f \left(\frac{e_f}{e}\right)^2 \frac{T^2\alpha\alpha_s}{8\pi^2} [f_q(\overrightarrow{p_\gamma}) + f_{\bar{q}}(\overrightarrow{p_\gamma})] \times \left[2\ln\left(\frac{4E_\gamma T}{m^2}\right) - C_{\rm ann} - C_{\rm Com}\right], \quad (37)$$

where T is the temperature, $C_{\rm ann} = 1.916$, and $C_{\rm Com} = 0.416$. It has been shown in Refs. [48,49], that the infrared dependence on the quark mass should be replaced by a dependence on the in-medium thermal quark mass, $m^2 = 2m_{\rm th}^2 = 4\pi\alpha_s T^2/3$. The phase-space distribution function of the incoming particles is

defined as follows:

$$g_i \int \frac{d^3x d^3p}{(2\pi)^3} f(x,\, p) = N_i, \tag{38}$$

where N_i is the number of particles i and g_i is the spin-color degeneracy. The phase-space distribution function for an incoming jet, assuming a Bjorken $\eta - y$ correlation [50], is as follows

$$\begin{aligned} f_{\rm jet}(\overrightarrow{x}\,,\,\overrightarrow{p}\,,t_0) &= \frac{(2\pi)^3\mathcal{P}(\mathbf{r}_\perp)}{g_q \tau p_T}\frac{dN^{\rm jet}}{dyd^2p_T}\delta(\eta - y) \\ &= \frac{(2\pi)^3\mathcal{P}(\mathbf{r}_\perp)t_0}{g_q\sqrt{t_0^2 - z_0^2}}\frac{p_T}{E^2}\frac{dN^{\rm jet}}{dyd^2p_T}\delta(z_0 - v_z t_0), \end{aligned} \tag{39}$$

where η is the space-time rapidity, t_0 is the formation time of the jet, and z_0 is its position in the QGP expansion direction. As before, the jets are taken to be massless and we suppose that energy loss of jets in the plasma does not change their direction. With this latter approximation, $f_{\rm jet}$ can be factorized into a position space and a momentum space part:

$$\begin{aligned} f_{\rm jet}(\overrightarrow{x}\,,\,\overrightarrow{p}\,,t) &= \chi(\overrightarrow{x}\,,t)\frac{1}{E^2}\frac{dN^{\rm jet}(E,t)}{dE} \\ &= \chi\left(\overrightarrow{x} - \hat{t}\frac{\overrightarrow{p}}{|\overrightarrow{p}|}, t_0\right)\frac{1}{E^2}\frac{dN^{\rm jet}(E,t)}{dE}, \end{aligned} \tag{40}$$

where $\hat{t} = t - t_0$ is the propagation time of the jet. In the high energy limit, the cross sections $\sigma_{q\bar{q}\to g\gamma}$ and $\sigma_{qg\to q\gamma}$ are dominated by direct exchange between the quark and the photons. Because we are interested in photons produced at midrapidity ($y = 0$), we only need to consider quark and antiquark jets produced at midrapidity. This gives the following:

$$f_{\rm jet}(\overrightarrow{x},\,\overrightarrow{p},t)\big|_{y=0} = \frac{(2\pi)^3\mathcal{P}(|\overrightarrow{w_r}|)t_0}{g_q\sqrt{t_0^2 - z_0^2}}\frac{1}{p_T}\frac{dN^{q\bar{q}}}{dyd^2p_T}(p_T,t)\delta(z_0), \tag{41}$$

where $\overrightarrow{w_r}$ is, in the plane $z_0 = 0$, the initial radial position of the jet,

$$\begin{aligned} |\overrightarrow{w_r}| &= \left(\overrightarrow{x} - \hat{t}\frac{\overrightarrow{p}}{|\overrightarrow{p}|}\right)\cdot\hat{r} \\ &= \sqrt{(r\cos\phi - t)^2 + r^2\sin^2\phi} \quad \text{for } t_0 \sim 0, \end{aligned} \tag{42}$$

and ϕ is the angle in the plane $z_0 = 0$ between the direction of the photon and the position where this photon has been produced. The AMY formalism is introduced here to calculate the evolution of $dN^{q\bar{q}}/dyd^2p_T(p_T,t)$. The output of Eq. (23) is $P_{q\bar{q}}(E,t)$, where

$$P_{q\bar{q}}(E,t) = \frac{dN^{q\bar{q}}}{dE}(E,t) \propto p_T\frac{dN^{q\bar{q}}}{dyd^2p_T}(p_T,t). \tag{43}$$

The initial distributions $P_{q\bar{q}}(E,t_0)$ and $P_g(E,t_0)$ are fixed by the initial jet distribution at midrapidity as parametrized in Ref. [39,40]. The total photon spectrum is given by a full space-time integration as follows:

$$\begin{aligned} \frac{dN^\gamma}{dyd^2p_T} &= \int d\tau\tau\int rdr\int d\phi \\ &\quad\times\int d\eta\frac{dR}{dyd^2p_T}[E_\gamma = p_T\cosh(y-\eta)] \\ &= \int dt\int rdr\int d\phi\int dz_0\frac{dR}{dyd^2p_T} \\ &\quad\times[E_\gamma = p_T\cosh(y_0)]. \end{aligned} \tag{44}$$

The production rate is calculated in the local frame where the temperature is defined where the photon rapidity becomes $y_0 = y - \eta$.

High-p_T photons are emitted preferentially early during the QGP phase, when the temperature is at its highest point. Indeed, explicit hydrodynamic calculations show that the nuclear space-time geometry smoothly evolves from 1D to 3D [51]. By the time the system reaches the temperature corresponding to the mixed phase in a first-order phase transition, the system is still very much 1D [51]. For such a geometry, specific calculations [52] suggest that the flow effect on photons and dileptons from the QGP is not large at RHIC and LHC for $p_T > 2$ GeV. Assuming again a 1D expansion, we get the production of photons from jet-medium interactions from Eqs. (37), (41), and (44),

$$\begin{aligned} \frac{dN^\gamma_{\rm jet-th}}{dyd^2p_T}\Big|_{y=0} &= 2\int dt\int_0^{R_\perp} rdr\int_0^\pi d\phi\frac{(2\pi)^3\mathcal{P}(|\overrightarrow{w_r}|)}{g_q} \\ &\quad\times\frac{1}{p_T}\frac{dN^{q\bar{q}}}{dyd^2p_T}(p_T,t)\sum_f\left(\frac{e_f}{e}\right)^2\frac{T^2\alpha\alpha_s}{8\pi^2} \\ &\quad\times\left[2\ln\left(\frac{3p_t}{\pi\alpha_s T}\right) - C_{\rm ann} - C_{\rm Com}\right], \end{aligned} \tag{45}$$

where the temperature T evolves according to Eq. (33). The ϕ integration can be done as follows:

$$\begin{aligned} &\int_0^\pi d\phi\mathcal{P}(|\overrightarrow{w_r}|) = \gamma(r,t) \\ &= \begin{cases} 0 & r^2 + t^2 - 2tr > R_\perp^2 \\ \frac{2}{R_\perp^2}\left(1 - \frac{r^2+t^2}{R_\perp^2}\right) & r^2 + t^2 + 2tr < R_\perp^2 \\ \frac{2u_0}{\pi R_\perp^2}\left(1 - \frac{r^2+t^2}{R_\perp^2}\right) + \frac{4tr}{\pi R_\perp^4}\sin(u_0) & \text{otherwise,} \end{cases} \end{aligned} \tag{46}$$

where

$$u_0 = \arccos\left(\frac{r^2 + t^2 - R_\perp^2}{2tr}\right). \tag{47}$$

Then, the final expression for the jet-photon production becomes the following:

$$\begin{aligned} \frac{dN^\gamma_{\rm jet-th}}{dyd^2p_T}\Big|_{y=0} &= 2\int dt\int_0^{R_\perp} rdr\frac{(2\pi)^3}{g_q}\frac{1}{p_T}\frac{dN^{q\bar{q}}}{dyd^2p_T} \\ &\quad\times(p_T,t)\gamma(r,t)\sum_f\left(\frac{e_f}{e}\right)^2\frac{T^2\alpha\alpha_s}{8\pi^2} \end{aligned}$$

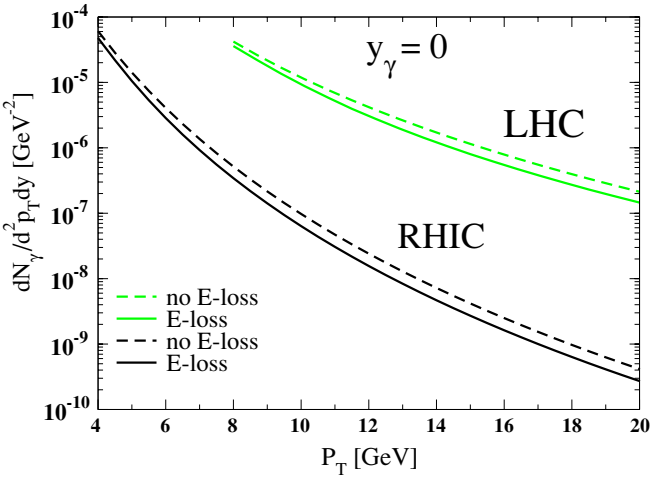

FIG. 11. (Color online) Direct production of photons by jets in the plasma for Au-Au at RHIC and Pb-Pb at the LHC. For the solid lines, jet energy loss is included; for the dashed lines it is neglected. The initial temperature is $T_i = 370$ MeV at RHIC and $T_i = 845$ MeV at the LHC.

$$\times \left[2 \ln \left(\frac{3 p_t}{\pi \alpha_s T} \right) - C_{\rm ann} - C_{\rm Com} \right] = \int dt \frac{dN^\gamma_{\rm jet-th}}{dt dy d^2 p_T} \Big|_{y=0}. \quad (48)$$

As before, we assume a first-order phase transition beginning at the time τ_f and ending at $\tau_H = r_d \tau_f$ [38]. After τ_f we scale the production rate by $f_{\rm QGP}$ [Eq. (34)] such that

$$\frac{dN^\gamma_{\rm jet-th}}{dy d^2 p_T}\Big|_{y=0} = \int_{\tau_i}^{\tau_f} dt \frac{dN^\gamma_{\rm jet-th}}{dt dy d^2 p_T}\Big|_{y=0} + \int_{\tau_f}^{\tau_H} dt f_{\rm QGP}(t) \frac{dN^\gamma_{\rm jet-th}}{dt dy d^2 p_T}\Big|_{y=0}. \quad (49)$$

The first term and second term correspond respectively to photons produced during the pure QGP and the mixed phase. Our results for RHIC and LHC, with and without energy loss are shown in Fig. 11. Here also, $\alpha_s = 0.3$. We see that higher energy photons are more sensitive to jet energy loss: photons at 4 GeV are suppressed by a factor 1.3 at RHIC, whereas 15 GeV photons are suppressed by a factor 1.6 because of jet energy loss. We find approximately the same suppression for the LHC. This suppression is much smaller that the one observed from R_{AA} in the previous section. This is because the photons can be produced at any point in the hard parton's propagation through the medium, whereas the jet energy loss depends on the final parton energy. Hence, some of the photon rate arises from before, rather than after, the jet has lost much energy.

B. Bremsstrahlung Photons

Hard partons in the medium can also produce photons by bremsstrahlung when they scatter in the medium. The photon bremsstrahlung rate $d\Gamma^{q\to q\gamma}(p,k)/dkdt$ follows the same expression as $d\Gamma^{q\to qg}(p,k)/dkdt$ in Eq. (19), but with $C_s \to e_f^2/e^2$, $C_A \to 0$, $m_\gamma = 0$, and $g_s^2 \to e^2$. The photon bremsstrahlung distribution is given by the following:

$$\frac{dP_\gamma(p,t)}{dt} = \int dk\ P_{q\bar{q}}(p+k) \frac{d\Gamma^{q\to q\gamma}(p+k,p)}{dkdt}. \quad (50)$$

It is assumed here that the photon production rate is so low that the quark plus antiquark distribution $P_{q\bar{q}}$ will be unchanged by the photon emission. The photon distribution is finally convolved with the initial spatial distribution of jets to get the final spectrum of bremsstrahlung photons,

$$\frac{dN_{\rm jet-br}}{dy d^2 p_T}\Big|_{y=0} = \frac{1}{p_T \Omega(y=0)} \frac{dN_{\rm jet-br}}{dp_T} = \frac{1}{p_T} \int d^2 r_\perp \mathcal{P}(\mathbf{r}_\perp) P_\gamma(p_T, d), \quad (51)$$

where $r_\perp$ is the position where the jet has been created and $d = d(r_\perp)$ is the distance crossed by the jet in the plasma. The factor $\Omega(y=0)$ corresponds to a $d\phi$ and a dy integration around the plane $y = 0$. This factor can be absorbed in the definition of the initial distribution $P_{q\bar{q}}(p_T, t=0)$.

Numerically, bremsstrahlung photons turn out to be subdominant to jet-photon conversion. This is because, whereas the rate at which such photons are produced is larger, they typically carry only a fraction of the jet's energy, whereas jet-photon conversion predominantly produces photons with the complete energy of the jet (hard parton). When folded against a steeply falling spectrum of jets, the process that produces the highest energy photons will dominate the final spectrum.

Recently, Zakharov has also considered bremsstrahlung emission of photons from jets [53]. His work accounts for finite-size effects in the high-energy limit; in this respect it is more complete than our work here. However, our energy range of interest for this study, as discussed at the end of Sec. III, is below the factorization scale, so finite size effects are small for the energies we consider.

C. Thermal photons

The thermal-thermal contribution comes from the photons produced by two scattering thermal particles. The Compton and annihilation rate has been calculated in the previous literature [48,49], and we use those results here. There are also leading order bremsstrahlung and inelastic pair annihilation contributions [54]; we use the parametrization for those rates presented there.

D. Nonthermal contributions

The expression for prompt photons produced in AA collisions is as follows:

$$\frac{dN_{\gamma-\rm prompt}}{dy d^2 p_T} = E_\gamma \frac{d\sigma}{d^3 p_\gamma} \frac{\langle N_{\rm coll}\rangle}{\sigma_{\rm in}}, \quad (52)$$

where we take the values $\langle N_{\rm coll}\rangle = 975$, $\sigma_{\rm in} = 40$ mb for RHIC [18] and $\langle N_{\rm coll}\rangle = 1670$, $\sigma_{\rm in} = 72$ mb for the LHC [55].

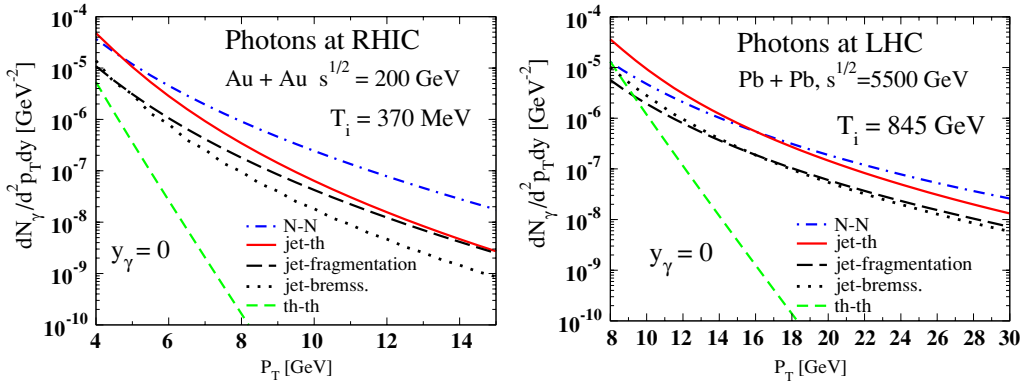

FIG. 12. (Color online) Contributing sources of high-p_T photons at midrapidity in central Au-Au collisions at RHIC (left panel) and Pb-Pb collisions at the LHC (right panel). (Solid line) Jet-photon conversion in the plasma; (dotted line) bremsstrahlung from jets in the plasma; (short dashed line) thermal induced production of photons; (long dashed line) fragmentation of jets outside the plasma; and (dot-dashed line) direct contribution from the primordial hard scattering.

$E_\gamma d\sigma/d^3p_\gamma$ is taken from Eq. (36) but with the photon fragmentation function accounting for the jet energy loss.

We assume, as we did for pion production, that photon production via fragmentation of a jet occurs after the jet parton leaves the QGP. Therefore, the photon fragmentation function, including the full spatial distribution and the secondary jets, is given by Eq. (29), with the substitution $\pi^0 \to \gamma$.

The preequilibrium contribution of photons, corresponding to photons emitted after the transit time of the two nuclei but before thermalization time, is not explicitly included in this work. However, a rough estimate might be had by choosing a smaller formation time, as we do. The modeling of those contributions is accessible by the parton cascade model [56]. Finally, to have a complete photon description, we have also calculated the background production, which mainly comes from the decay $\pi^0 \to \gamma\gamma$. This is given by [57] the following:

$$\frac{dN_{\gamma-\mathrm{BG}}}{dyd^2p_T} = \int dy^{\pi^0} d^2p_T^{\pi^0} \frac{dN^{\pi^0}}{dy^{\pi^0}d^2p_T^{\pi^0}} \frac{dP(\mathbf{p}_{\pi^0} \to \mathbf{p}_\gamma)}{dyd^2p_T}. \quad (53)$$

All the previous procedures for jet energy loss, initial spatial distribution and the effect of secondary jets are included in the calculation of the pion spectrum $dN^{\pi^0}/dy^{\pi^0}d^2p_T^{\pi^0}$. In the pion center-of-mass frame, the photon distribution is given by the following:

$$\frac{dP(\mathbf{p}_{\pi^0} \to \mathbf{p}_\gamma)}{dyd^2p_T} = \frac{\delta\left(E^\gamma_{\mathrm{cm}} - \frac{m_{\pi^0}}{2}\right)}{2\pi E^\gamma_{\mathrm{cm}}}, \quad (54)$$

where

$$E^\gamma_{\mathrm{cm}} = p_T \cosh y \sqrt{\sin^2\theta + \frac{(E_{\pi^0}\cos\theta - |\mathbf{p}_{\pi^0}|)^2}{m^2_{\pi^0}}} \quad (55)$$

and θ is the angle between $\mathbf{p}_{\pi^0}$ and $\mathbf{p}_\gamma$. With the η branching ratio $\Gamma^{\eta\to\gamma\gamma}/\Gamma^\eta \sim 40\%$ [58] and its relative yield $N^\eta/N^{\pi^0} \sim 0.5$ [59], we simply multiply Eq. (54) by a factor of 1.2 to include the η contribution.

E. Results

Each contribution of high p_T photons, except the background, are shown in Fig. 12 for central collisions at RHIC and the LHC. The energy loss is included in all processes involving jets. Prompt photons have been split into the direct component (*N-N*) and the fragmentation component. All those processes, except the contribution from jet-medium bremsstrahlung, have been presented in Ref. [39] for the case of no energy loss. For RHIC, as in Ref. [39], the high p_T region is dominated by direct photons. However, in Ref. [39], the jet-photon conversion was dominant below 6 GeV, whereas in our study, direct photons dominate all the high p_T spectrum. A few factors explain this difference. The jet energy loss is included here; the constants C_{ann} and C_{Com} appearing in Eq. (37) have been set equal to 1.916 in Ref. [39]; the K_{jet} factor in the original publication is larger than ours: $K_{\mathrm{jet}} = 2.5$ is used for both RHIC and the LHC, whereas we use $K_{\mathrm{jet}} = 1.7$ for RHIC and 1.6 for LHC. Finally, no K_γ factor has been used for the direct contribution in Ref. [39]. It is, however, satisfying that the inclusion of jet energy loss does not spoil the original premise: jet-photon conversion is an important source of electromagnetic radiation.

At the LHC, our result is dominated by direct photons for p_T above 20 GeV, but there is a window, below 14 GeV, where the jet-photon conversion in the plasma is the dominant mechanism of photon production. In Ref. [39], however, the jet fragmentation (called bremsstrahlung in their study) was the most important process at the LHC, but jet suppression was not included. Photon production via jet bremsstrahlung in the plasma (dotted lines) turns out to be weak, but nonnegligible. It is approximately a factor of 3 below the jet-photon conversion contribution. Finally, the thermal induced photons (short dashed lines) are far below all other contributions in intensity.

New results for total photon production, after background subtraction, are now available [60]. Our calculations are compared to experimental data on the left-hand side of Fig. 13. The solid line includes the prompt photon contribution (pQCD), the QGP (jet-th, th-th, and jet-bremss.) and hadron gas contribution, extracted from Ref. [41]. This latter

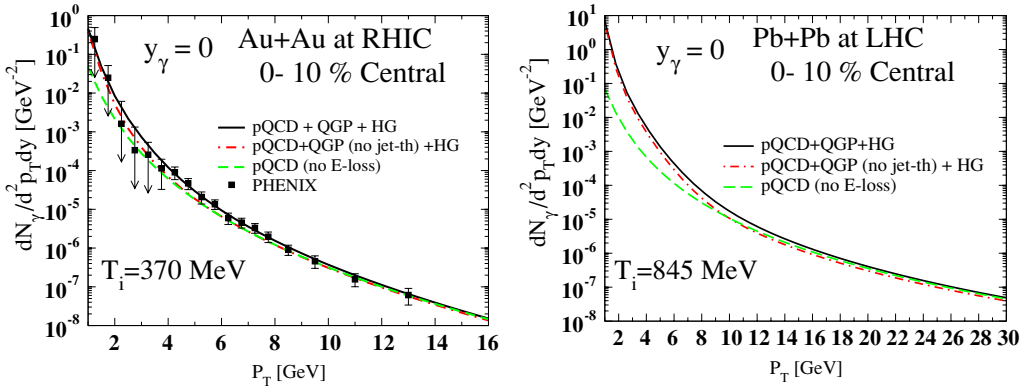

FIG. 13. (Color online) Total production of photons in central Au-Au collisions at RHIC and Pb-Pb at the LHC. The solid lines include all process from Fig. 12 and the hadron gas contribution [41], whereas the dot-dashed lines do not include the jet-thermal contribution. *p-p* collisions scaled to *A-A* are shown by the dashed lines. Data at RHIC are from PHENIX [60].

contribution becomes important only for $p_T < 1.5$ GeV. The initial condition for the thermal phase corresponds to $T_i = 370$ MeV and $\tau_i = 0.26$ fm/c. For a better comparison with data, we have extended our calculation down to $p_T = 1$ GeV. No cutoff has been applied on either jet-th or pQCD process. NLO calculations are not very reliable is this region, but thermal induced reactions and hadron gas contributions turn out to dominate here and NLO results play a minor role. When the jet-photon conversion is not included (dot-dashed line), the total photon production is reduced by up to 45%, around $p_T = 3$ GeV, showing the importance of that process. The result expected from *N-N* collisions scaled to Au-Au is also shown (dashed line). The plasma contribution, especially the jet-thermal process, is very important for $p_T < 6$ GeV. However, large error bars prevent a strong claim about the presence of a QGP.

Figure 14 shows the QGP photons for three different initial conditions: ($T_i = 447$ MeV, $\tau_i = 0.147$ fm/c), ($T_i = 370$ MeV, $\tau_i = 0.26$ fm/c), and ($T_i = 280$ MeV, $\tau_i = 0.6$ fm/c). As the high-p_T photons are produced early in the collision, they may be affected by the initial conditions. However, the high-p_T region is dominated by jet-therm processes, which are weakly sensitive to (T_i, τ_i), because the jet distribution function f_{jet} has a weak temperature dependence. We see that going from $\tau_i = 0.6$ fm/c to $\tau_i = 0.26$ fm/c increases the photon production in the QGP phase by less that a factor of 2; this additional contribution could be interpreted in some sense as a preequilibrium contribution.

Our prediction for the LHC is shown in the right-hand side of Fig. 13. The signature of the QGP phase is much stronger than at RHIC, increasing the photon yield, relatively to *N-N* scaled to *A-A* collision, by one order of magnitude around $p_T = 3$ GeV, where the hadron gas contribution turns out to be negligible.

Finally, we have calculated the ratio of the total number of photons and the background photons

$$\gamma_{\text{Total}}/\gamma_{\text{BG}} = \frac{\frac{dN_{\gamma-\text{BG}}}{d^2p_T dy} + \sum \text{all other sources}}{\frac{dN_{\gamma-\text{BG}}}{d^2p_T dy}} \qquad (56)$$

and compared in Fig. 15, with the result from PHENIX [61], with and without the QGP contribution. The calculation, including the QGP contribution is in agreement with the data from RHIC, except for a few data points in the range $7 < p_T < 9$ GeV. Without the thermal contributions, the resulting line (dot-dashed) does not overlap at all with the experimental data. That could constitute a signature of the importance of the jet-photon conversion inside the QGP, because this is the most important thermal process as we have seen in Fig. 12. We also show the weak effect of the initial temperature. The ratio $\gamma_{\text{Total}}/\gamma_{\text{BG}}$ at $T_i = 447$ MeV is only enhanced by $\sim 5\%$ relatively to the result at $T_i = 370$ MeV. Finally at the LHC (right panel), the thermal contribution is also visible; including the photons from the thermal phase enhances the calculation by $\sim$15%.

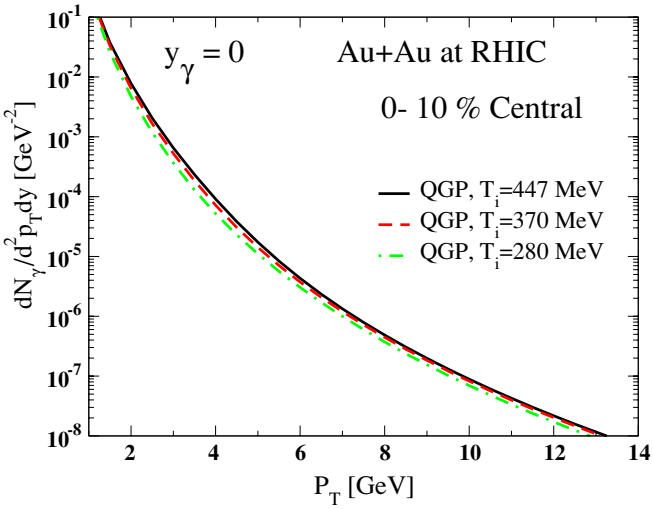

FIG. 14. (Color online) Production of photons during the QGP phase for three QGP initial conditions: (solid line) $T_i = 447$ MeV, $\tau_i = 0.147$ fm/c; (dashed line), $T_i = 370$ MeV, $\tau_i = 0.26$ fm/c; and (dot-dashed line) $T_i = 280$ MeV, $\tau_i = 0.6$ fm/c.

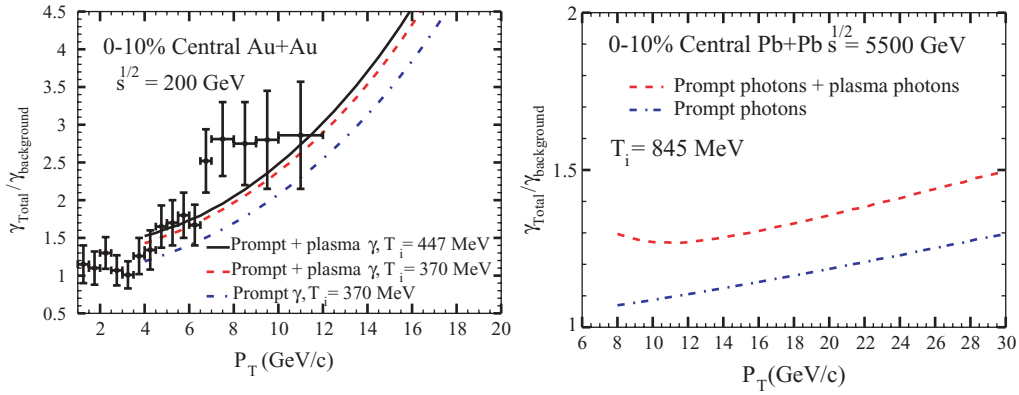

FIG. 15. (Color online) Ratio of all photons over all decay photons as a function of p_T, in Au-Au collisions at RHIC (left panel) and Pb-Pb at the LHC (right panel), with and without the thermal contribution. In the left panel, the effect of the initial temperature is also shown. The data are from the PHENIX [61] collaboration.

VI. SUMMARY AND CONCLUSIONS

We have used a complete leading order treatment of jet energy loss in the QCD plasma to calculate the pion and photon spectra for both RHIC and the LHC. The calculations have been confronted with available data from RHIC and turn out to be in good agreement. These results reinforce the idea that high p_T suppression is a final state effect caused by jet energy loss through bremsstrahlung in the hot medium.

The neutral pion nuclear modification factor at RHIC has been reproduced with an initial temperature $T_i = 370$ MeV and a formation time $\tau_i = 0.26$ fm/c, corresponding to $dN/dy = 1260$. Those parameters are consistent with the analysis in Ref. [41]. R_{AA} has shown a large dN/dy dependence, but a weak dependence on the initial temperature T_i (provided the starting time τ_i is changed to keep dN/dy constant). The calculation included the nuclear geometry; assuming that all jets are produced at the center overestimates the suppression by $\sim$50%.

We have also computed the production of high p_T photons from the initial collision, from the medium, and from jet-medium interactions. The jet-medium photons improve the agreement between experiment and theory at RHIC, and they are expected to dominate the signal at the LHC below about 14 GeV. Thermal photons from the medium are not very important to either experiment, in the kinematical range on which we have concentrated. In light of these results, the in-medium production of dileptons should also be reconsidered. Work on this topic, and others, is in progress.

ACKNOWLEDGMENTS

We thank P. Aurenche, R. J. Fries, J. S. Gagnon, B. Müller, and D. K. Srivastava for useful communications. This work was supported in part by the Natural Sciences and Engineering Research Council of Canada and, in part, for S.T., C.G. and S.J. by le Fonds Nature et Technologies du Québec. S.J. also thanks RIKEN BNL Center and U.S. Department of Energy [DE-AC02-98CH10886] for providing facilities essential for the completion of this work.

[1] F. Karsch, Nucl. Phys. **A698**, 199 (2002).
[2] S. S. Adler *et al.*, Phys. Rev. Lett. **91**, 072301 (2003).
[3] J. Adams *et al.*, Phys. Rev. Lett. **91**, 172302 (2003).
[4] C. Adler *et al.*, Phys. Rev. Lett. **90**, 082302 (2003).
[5] J. P. Blaizot and F. Gelis, Nucl. Phys. **A750**, 148–165 (2005).
[6] X. N. Wang, Phys. Rev. C **63**, 054902 (2001).
[7] M. Gyulassy, I. Vitev, and X. N. Wang, Phys. Rev. Lett. **86**, 2537 (2001).
[8] M. Gyulassy and M. Plümer, Phys. Lett. **B243**, 432 (1990).
[9] X. N. Wang, M. Gyulassy, and M. Plümer, Phys. Rev. D **51**, 3436 (1995).
[10] A. B. Migdal, Phys. Rev. **103**, 1811 (1956).
[11] R. Baier, Y. L. Dokshitzer, A. H. Mueller, S. Peigné, and D. Schiff, Nucl. Phys. **B484**, 291 (1997).
[12] R. Baier, Y. L. Dokshitzer, A. H. Mueller, and D. Schiff, J. High Energy Phys. 09 (2001) 033.
[13] M. Gyulassy, P. Levai, and I. Vitev, Phys. Rev. Lett. **85**, 5535 (2000); Nucl. Phys. **B594**, 371 (2001).
[14] A. Kovner and U. A. Wiedemann, "Gluon radiation and parton energy loss," in *Quark Gluon Plasma*, edited by R. C. Hwa (World Scientific, Singapore, 2003), p. 192.
[15] B. G. Zakharov, JETP Lett. **63**, 952 (1996); **70**, 176 (1999); **65**, 615 (1997); Phys. Atom. Nucl. **61**, 838 (1998).
[16] X. N. Wang and M. Gyulassy, Phys. Rev. Lett. **68**, 1480 (1992).
[17] X. N. Wang, Z. Huang, and I. Sarcevic, Phys. Rev. Lett. **77**, 231–234 (1996).
[18] S. Jeon, J. J. Marian, and I. Sarcevic, Phys. Lett. **B562**, 45 (2003).
[19] M. Gyulassy, I. Vitev, X. N. Wang, and B. W. Zhang, in *Quark Gluon Plasma*, edited by R. C. Hwa (World Scientific, Singapore, 2003).
[20] P. Arnold, G. D. Moore, and L. Yaffe, J. High Energy Phys. 11 (2001) 057; 06 (2002) 030.

[21] K. Adcox *et al*., submitted to Nucl. Phys. **A**; nucl-ex/0410003.
[22] S. S. Adler *et al*. (PHENIX Collaboration), Phys. Rev. C **69**, 034910 (2004).
[23] S. Jeon and G. D. Moore, Phys. Rev. C **71**, 034901 (2005).
[24] R. Baier, D. Schiff, and B. G. Zakharov, Annu. Rev. Nucl. Part. Sci. **50**, 37–69 (2000).
[25] J. Adams *et al*. (STAR Collaboration), Phys. Rev. Lett. **91**, 072304 (2003).
[26] P. Aurenche, F. Gelis, and H. Zaraket, J. High Energy Phys. 05 (2002) 043.
[27] E. Wang and X. N. Wang, Phys. Rev. Lett. **87**, 142301 (2001).
[28] J. F. Owens, Rev. Mod. Phys. **59**, 465 (1987).
[29] G. Barnaföldi, G. Fai, P. Lévai, G. Papp and Y. Zhang, J. Phys. G: Nucl. Part. Phys. **27**, 1767 (2001).
[30] H. L. Lai, J. Huston, S. Kuhlmann, J. Morfin, F. Olness, J. F. Owens, J. Pumplin, and W. K. Tung, Eur. Phys. J. C **12**, 375 (2000).
[31] J. Binnewies, B. A. Kniehl, and G. Kramer, Phys. Rev. D **52**, 4947 (1995).
[32] S. S Adler *et al*., Phys. Rev. Lett. **91**, 241803 (2003).
[33] R. J. Fries, B. Müller, C. Nonaka, and S. A. Bass, Phys. Rev. C **68**, 044902 (2003).
[34] K. J. Eskola, V. J. Kolhinen, and C. A. Salgado, Eur. Phys. J. C **9**, 61 (1999).
[35] X. N. Wang, Phys. Lett. **B579**, 299 (2004).
[36] H. Niemi, S. S. Räsänen, and P. V. Ruuskunen, contribution to [54].
[37] M. Gyulassy, I. Vitev, X. N. Wang, and P. Huovinen, Phys. Lett. **B526**, 301 (2002).
[38] J. D. Bjorken, Phys. Rev. D **27**, 140 (1983).
[39] R. J. Fries, B. Müller, and D. K. Srivastava, Phys. Rev. Lett **90**, 132301 (2003).
[40] D. K. Srivastava, C. Gale, and R. J. Fries, Phys. Rev. C **67**, 034903 (2003).
[41] S. Turbide, R. Rapp, and C. Gale, Phys. Rev. C **69**, 014903 (2004).
[42] J. Kapusta, L. D. McLerran, and D. K. Srivastava, Phys. Lett. **B283**, 145 (1992).
[43] T. Hirano and Y. Nara, Phys. Rev. C **69**, 034908 (2004).
[44] P. Aurenche, R. Baier, A. Douiri, M. Fontannaz, and D. Schiff, Nucl. Phys. **B286**, 553 (1987); **297**, 661 (1988).
[45] M. Gluck, E. Reya, and A. Vogt, Phys. Rev. D **48**, 116 (1993); Erratum: *ibid*. **51**, 1427 (1995); L. Bourhis, M. Fontannaz, and J. Ph. Guillet, Eur. Phys. J. C. **2**, 529 (1998).
[46] K. Reygers, talk at the Intern. Conf. on Hard Probes of High Energy Nuclear Collisions, Lisbon, Portugal, 2004.
[47] C. Y. Wong, *Introduction to High-Energy Heavy Ion Collisions* (World Scientific, Singapore, 1994).
[48] J. Kapusta, P. Lichard, and D. Seibert, Phys. Rev. D **44**, 2774 (1991).
[49] R. Baier, H. Nakkagawa, A. Niegawa, and K. Redlich, Z. Phys. C **53**, 433 (1992).
[50] Z. Lin and M. Gyulassy, Phys. Rev. C **51**, 2177 (1995).
[51] P. F. Kolb and W. Heinz, "Hydrodynamic description of Ultrarelativistic Heavy ion collisions," in *Quark Gluon Plasma*, edited by R. C. Hwa (World Scientific, Singapore, 2003), p. 634; nucl-th/0305084.
[52] D. K. Srivastava, M. G. Mustafa, and B. Müller, Phys. Rev. C **56**, 1064 (1997).
[53] B. G. Zakharov, JETP Lett. **80**, 1 (2004).
[54] P. Arnold, G. D. Moore, and L. G. Yaffe, J. High-Energy Phys. 12 (2001) 009.
[55] F. Arleo *et al*., *Photon Physics in Heavy Ion Collisions*, Cern yellow book report, hep-ph/0311131.
[56] S. A. Bass, B. Muller, and D. K. Srivastava, Phys. Rev. Lett. **90**, 082301 (2003).
[57] R. N. Cahn, Phys. Rev. D **7**, 247 (1973).
[58] S. Eidelman *et al*. (Particle Data Group), Phys. Lett. **B592**, 1 (2004).
[59] R. Albrecht *et al*., Phys. Lett. **B361**, 14 (1995).
[60] S. S. Adler *et al*., submitted to Phys. Rev Lett. nucl-ex/0503003.
[61] J. Frantz *et al*., J. Phys. G Nucl. Part. Phys. **30**, s1003 (2004).